Model Predictive Control for Very Flexible Aircraft Based on Linear Parameter Varying Reduced-Order Models

Conference Paper · June 2022

CITATIONS
0

READS
69

5 authors, including:

Mateus de Freitas Virgilio Pereira
University of Michigan
24 PUBLICATIONS **66** CITATIONS
SEE PROFILE

Molong Duan
The Hong Kong University of Science and Technology
30 PUBLICATIONS **262** CITATIONS
SEE PROFILE

Carlos E. S. Cesnik
University of Michigan
340 PUBLICATIONS **11,008** CITATIONS
SEE PROFILE

International Forum on Aeroelasticity and Structural Dynamics
IFASD 2022
13-17 June 2022, Madrid, Spain

MODEL PREDICTIVE CONTROL FOR VERY FLEXIBLE AIRCRAFT BASED ON LINEAR PARAMETER VARYING REDUCED-ORDER MODELS

Mateus F. V. Pereira[1], Molong Duan[1], Carlos E. S. Cesnik[1], Ilya Kolmanovsky[1], Fabio Vetrano[2]

[1]University of Michigan
{mfvp,molong,cesnik,ilya}@umich.edu

[2]Airbus Operations S.A.S.
fabio.vetrano@airbus.com

Keywords: Maneuver Load Alleviation, Very Flexible Aircraft, Model Predictive Control, Reduced-Order Model, Linear Parameter Varying Model

Abstract: This paper presents the design of an active maneuver load alleviation (MLA) system for very flexible aircraft (VFA) using a linear parameter varying reduced-order model (ROM) referred to as the top-to-bottom ROM (T2B-ROM). This model is obtained by constructing a piecewise-linear model as a function of the altitude and Mach number, and then reducing it using local bases computed by balanced truncation. The controller is based on a Model Predictive Control (MPC) architecture. Constraints are enforced to keep the bending loads within desired bounds. The controller design is verified via nonlinear numerical simulations.

1 INTRODUCTION

Model predictive control (MPC) architectures for automatic flight control design with maneuver load alleviation (MLA) capabilities have shown to be successful in achieving command tracking and enforcing constraints to keep loads within prescribed limits in very flexible aircraft (VFA) [1, 2]. Models for such kind of vehicles usually come from finite-element solutions, therefore one of the challenges of implementing the MPC-based MLA systems is the computational cost to use high-dimensional systems for prediction in real time. For this reason, model order reduction techniques are usually applied to create a low-cost model that approximates the behavior of the original system.

In the work of Lanchares et al. [3], a linear parameter varying reduced-order model (ROM) referred to as the top-to-bottom ROM (T2B-ROM) was introduced. This model is obtained by constructing a piecewise-linear model as a function of the altitude and Mach number, and then reducing it using local bases computed by balanced truncation. The resulting ROM is a hybrid system with continuous dynamics in each individual reduced-order subspace with no state jump in switching. The T2B-ROM has been shown to provide a good approximation of the VFA dynamics.

This paper investigates the use of T2B-ROMs to develop an MPC-based MLA system for a very flexible commercial aircraft model. The prediction model utilizes the T2B-ROM to capture changes in the dynamics and to avoid future constraint violations. In particular, constraints are enforced on the out-of-plane curvature at critical stations to keep the bending loads within the

desired bounds, following the idea presented in the work of Pereira et al. [1, 2] in which shape control is used to alleviate in-flight loads.

2 TOP-TO-BOTTOM MODEL

Lanchares et al. [3] introduced a Top-to-bottom (T2B) reduced-order model for creating a nonlinear ROM. The ROM is obtained by constructing a piecewise-linear surrogate model in continuous time and then reducing it using local bases computed by balanced truncation. The resulting ROM is a hybrid system with continuous dynamics corresponding to the evolution within each individual set of reduced-order bases. The T2B ROM has shown to provide a good approximation for the dynamics of VFA.

Consider a model for VFA represented by the following nonlinear equations:

$$\dot{x} = f(x,u), \tag{1}$$
$$y = g(x,u), \tag{2}$$

where $x \in \mathbb{R}^{n_x}$ is the state vector, $u \in \mathbb{R}^{n_u}$ is the input vector, $y \in \mathbb{R}^{n_y}$ is the output vector, and $f : \mathbb{R}^{n_x} \times \mathbb{R}^{n_u} \to \mathbb{R}^{n_x}$ and $g : \mathbb{R}^{n_x} \times \mathbb{R}^{n_u} \to \mathbb{R}^{n_y}$ are continuously differentiable functions.

Given a pair $(x^i, u^i) \in \mathbb{R}^{n_x} \times \mathbb{R}^{n_u}$, a first-order local approximation of the nonlinear system in the neighborhood $(x,u) \in B_{(x^i,u^i)}(\varepsilon),\ \varepsilon \geq 0$, is given by:

$$\dot{x} \approx f(x^i,u^i) + \left.\frac{\partial f(x,u)}{\partial x}\right|_{(x^i,u^i)} (x - x^i) + \left.\frac{\partial f(x,u)}{\partial u}\right|_{(x^i,u^i)} (u - u^i), \tag{3}$$
$$= K_i + A_i x + B_i u \tag{4}$$
$$y \approx g(x^i,u^i) + \left.\frac{\partial g(x,u)}{\partial x}\right|_{(x^i,u^i)} (x - x^i) + \left.\frac{\partial g(x,u)}{\partial u}\right|_{(x^i,u^i)} (u - u^i) \tag{5}$$
$$= L_i + C_i x + D_i u, \tag{6}$$

where

$$A_i = \left.\frac{\partial f(x,u)}{\partial x}\right|_{(x^i,u^i)},\ B_i = \left.\frac{\partial f(x,u)}{\partial u}\right|_{(x^i,u^i)},\ K_i = f(x^i,u^i) - A_i x^i - B_i u^i \tag{7}$$
$$C_i = \left.\frac{\partial g(x,u)}{\partial x}\right|_{(x^i,u^i)},\ D_i = \left.\frac{\partial g(x,u)}{\partial u}\right|_{(x^i,u^i)},\ L_i = g(x^i,u^i) - C_i x^i - D_i u^i \tag{8}$$

The system in Eqs. 4-6 is referred to as the linearized system and is denoted by $\mathcal{S}_i$. Now consider a collection of M pairs $\mathcal{M} = \{(x^i,u^i) \in \mathbb{R}^{n_x} \times \mathbb{R}^{n_u}, i = 1,\ldots,M\}$ and their associated linearized systems. Then, the nonlinear system is approximated in the region defined by the convex hull of $\mathcal{M}$, $\mathrm{conv}(\mathcal{M})$, by the convex combination of the linearized models (i.e., $\mathcal{S}_i,\ i = 1,\ldots,M$) as follows:

$$\dot{x} = f(x,u) \approx \sum_{i=1}^{M} w_i(x,u)\left(K_i + A_i x + B_i u\right), \tag{9}$$
$$y = g(x,u) \approx \sum_{i=1}^{M} w_i(x,u)\left(L_i + C_i x + D_i u\right), \tag{10}$$

where w_i are interpolation weights satisfying

$$\sum_{i=1}^{N} w_i(x,u) = 1, \tag{11}$$

$$w_i(x,u) \geq 0,\ i = 1,\ldots,M. \tag{12}$$

These weights are defined based on the distance defined over a subset of outputs representing the flight conditions. Define the subsets of the output to be ζ; ζ_i represents its value at the selected linearization point of linearized system $\mathcal{S}_i$. The weights are defined using distance function $d_i(x,u)$ as

$$w_i(x,u) = \frac{e^{-\beta_d d_i(x,u)/m(x,u)}}{\sum_{j=1}^{N} e^{-\beta_d d_j(x,u)/m(x,u)}}, \tag{13}$$

where

$$d_i(x,u) = ||\zeta - \zeta_i||_2, \quad m(x,u) = \min_i d_i(x,u). \tag{14}$$

Note that the conditions specified in Eq. 12 are satisfied by the definitions of Eq. 13.

The linearization points correspond to different values of altitude (h) and Mach number (M), i.e., $\zeta = [h\ \ M]^T$. For each one of them, the corresponding pair (x_i, u_i) is a trimmed state-input. The linearized systems are then obtained for each one of these flight conditions to capture the change in dynamics within the specified flight envelope.

Each linearized model $\mathcal{S}_i$ generated may have more than 1000 states. Such a high number of states can preclude MPC applications due to the high computational cost. Therefore, model order reduction is performed through balanced truncation. This projection-based technique relies on the assumption that the state of the $\mathcal{S}_i$ system in Eqs. 4-6 evolves within a reduced-order subspace $D_p^i \subset \mathbb{R}^{n_x}$ of the original system. Let n_r be the dimension of D_p^i.

The subset D_p^i passing through an arbitrary $x^0 \in \mathbb{R}^{n_x}$ is defined by the triple (x^0, V_i, W_i), where $V_i, W_i \in \mathbb{R}_{n_x \times n_r}$ are projection matrices. Define the reduced-order linearized dynamics to be $\mathcal{S}_{r,i,j}$, where the subscript in $\mathcal{S}_{r,i,j}$ means that the reduced-order model was created by projecting the dynamics of system $\mathcal{S}_i$ onto the subspace D_p^j generated by the balance truncation of system $\mathcal{S}_j$. Accordingly, $\mathcal{S}_{r,i,j}$ is given by:

$$\dot{x}_r = P_j K_i + P_j A_i (I - V_j P_j) x^0 + P_j A_i V_j x_r + P_j B_i u \tag{15}$$

$$= K_{r,i,j} + A_{r,i,j} x_r + B_{r,i,j} u, \tag{16}$$

$$y = L_i + C_i (I - V_j P_j) x^0 + C_i V_j x_r + D_i u \tag{17}$$

$$= L_{r,i,j} + C_{r,i,j} x_r + D_{r,i,j} u, \tag{18}$$

$$\tag{19}$$

where x^0 is the initial condition of the full-order $\mathcal{S}_i$ model and

$$P_j = (W_j^T V)^{-1} W_j^T, \tag{20}$$

$$K_{r,i,j} = P_j K_i + P_j A_i (I - V_j P_j) x^0,\ A_{r,i,j} = P_j A_i V_j,\ B_{r,i,j} = P_j B_i, \tag{21}$$

$$L_{r,i,j} = L_i + C_i (I - V_j P_j) x^0,\ C_{r,i,j} = C_i V_j,\ D_{r,i,j} = D_i. \tag{22}$$

Therefore, for M linearization points, M^2 reduced-order models are created. For models in the jth subspace, that is, $\mathcal{S}_{r,i,j}$ for $i = 1, \ldots, M$, an interpolation similar to the one in Eqs. 9 and 10 is performed to provide a reduced-order approximation of the original nonlinear system on such subspace:

$$\begin{aligned}
\dot{x}_r &= P_j f(V_j x_r + (I - V_j P_j)x^0, u) && (23)\\
&\approx \sum_{i=1}^{M} w_i(V_j x_r + (I - V_j P_j)x^0, u)\,(K_{r,i,j} + A_{r,i,j}x_r + B_{r,i,j}u) && (24)\\
y &= g(V_j x_r + (I - V_j P_j)x^0, u) && (25)\\
&\approx \sum_{i=1}^{M} w_i(V_j x_r + (I - V_j P_j)x^0, u)\,(L_{r,i,j} + C_{r,i,j}x_r + D_{r,i,j}u)\,, && (26)
\end{aligned}$$

As the system evolves in time, the distance between the full-order state x and the different subspaces D_p^j for $j = 1, \ldots, M$ varies, as shown in Fig. 1. The closest the subspace is from the current state, the better reduced-order approximation it can provide. Therefore, it is reasonable to switch to the closest subspace, that is, update matrices V_j and W_j in Eqs. 24-26 based on the following rule:

$$j \in \{0, 1, \ldots, M\} \text{ such that } m(x_r, u) = d_j(V_j x_r + (I - V_j P_j)x^0, u), \qquad (27)$$

where $m(\cdot)$ and $d(\cdot)$ are given in Eq. 14. The piecewise-linear reduced-order system in Eqs. 24-26 along with the switching rule in Eq. 27 are referred to as the T2B-ROM. Figure 2 depicts the schematic operation of such a model. Note that the reduced-order models and their respective bases are computed off-line, thus making the evaluation of the T2B-ROM cheaper than the original nonlinear system.

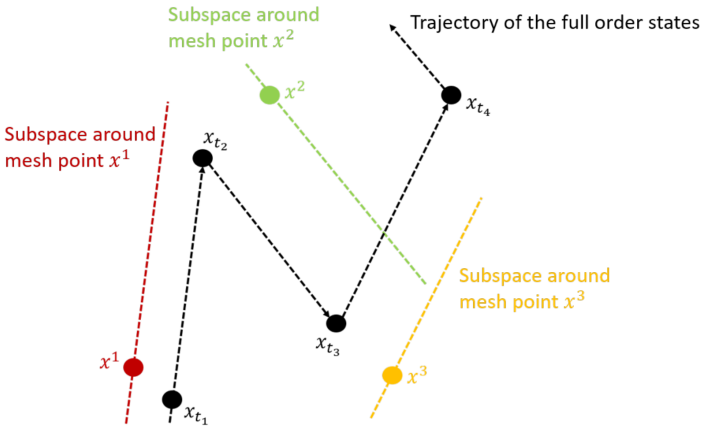

Figure 1: Graphical illustration of the piecewise-linear ROM [3].

For control design purposes, it is useful to define the T2B-ROM as a function of the variation of x_r from the projected initial condition. By applying the following change of coordinates to each system $\mathcal{S}_i$

$$\begin{aligned}
\delta x &= x - x^i && (28)\\
\delta u &= u - u^i && (29)\\
\delta y &= y - g(x^i, u^i) && (30)\\
& && (31)
\end{aligned}$$

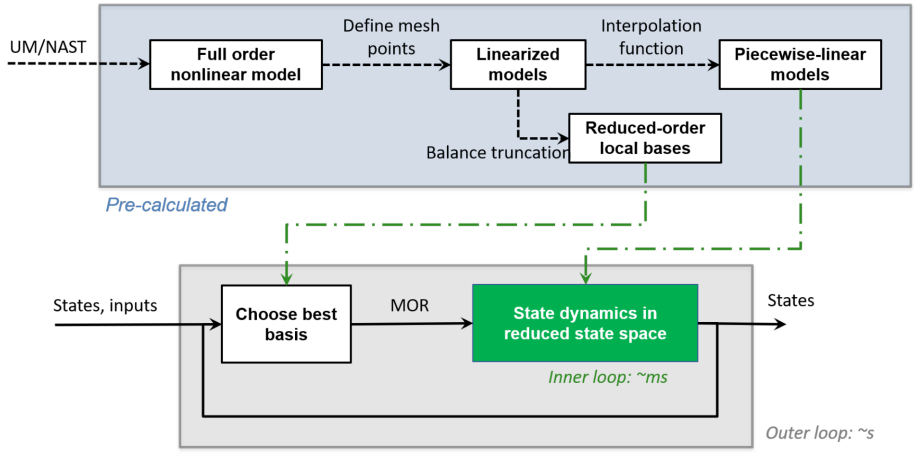

Figure 2: Schematic operation of piecewise-linear ROM algorithm [3].

and then building the reduced-order model following the aforementioned procedure, the following T2B-ROM is obtained:

$$\delta\dot{x}_r \approx \sum_{i=1}^{M} w_i(V_j\delta x_r + (I + P_j - V_jP_j)x^0, u)\,(A_{r,i,j}\delta x_r + B_{r,i,j}\delta u) \tag{32}$$

$$\delta y \approx \sum_{i=1}^{M} w_i(V_j\delta x_r + (I + P_j - V_jP_j)x^0, u)\,(C_{r,i,j}\delta x_r + D_{r,i,j}\delta u)\,, \tag{33}$$

$$j \in \{0, 1, \ldots, M\} \text{ such that } m(x_r, u) = d_j(V_j\delta x_r + (I + P_j - V_jP_j)x^0, u). \tag{34}$$

where

$$\delta x_r = x_r - P_j x^0. \tag{35}$$

3 AIRCRAFT MODEL

The XRF1 is an Airbus provided industrial standard multi-disciplinary research testcase representing a typical configuration for a long range wide body aircraft. The XRF1 research testcase is used by Airbus to engage with external partners on development and demonstration of relevant capabilities/technologies. To create a model that represents a flexible aircraft with increased flexibility, the Airbus-Michigan Center for Aero-Servo-Elasticity of Very Flexible Aircraft (CASE-VFA) modified the baseline XRF1 to create XRF1-HARW [4], a model for a future high-aspect-ratio-wing commercial transport vehicle. XRF1-HARW has the same geometry and properties as XRF1, but with a wing 20% longer. Therefore, the nonlinear effects become more pronounced, and the flexible and rigid body responses can have frequencies of similar magnitude. In fact, the first out-of-plane bending moment of XRF1-HARW is 40.26% smaller than the same frequency of the baseline XRF1.

The University of Michigan's Nonlinear Aeroelastic Simulation Toolbox (UM/NAST) [5] was the main tool utilized to design and simulate the XRF1-HARW model. It employs geometrically nonlinear strain based finite elements, different options for steady and unsteady aerodynamics, and nonlinear 6-degree of freedom (DOF) rigid body equations of motion to numerically simulate the dynamics of the aircraft.

Based on the UM/NAST model, a T2B-ROM representation was created for the XRF1-HARW test case. The model was linearized at different values of altitude and Mach number, as shown

in Tab. 1. Each pair (h_i, M_i) is identified by a number from 1 to 96. The linearized systems were then obtained using the complex-step differentiation method in UM/NAST.

Table 1: Linearization points of XRF1-HARW and their respective label.

		Mach					
		0.80	**0.81**	**0.82**	**0.83**	**0.84**	**0.85**
Altitude [m]	**8000**	1	2	3	4	5	6
	8100	7	8	9	10	11	12
	8200	13	14	15	16	17	18
	8300	19	20	21	22	23	24
	8400	25	26	27	28	29	30
	8500	31	32	33	34	35	36
	8600	37	38	39	40	41	42
	8700	43	44	45	46	47	48
	8800	49	50	51	52	53	54
	8900	55	56	57	58	59	60
	9000	61	62	63	64	65	66
	9100	67	68	69	70	71	72
	9200	73	74	75	76	77	78
	9300	79	80	81	82	83	84
	8400	85	86	87	88	89	90
	9500	91	92	93	94	95	96

Each linearized model $\mathcal{S}_i$ generated by UM/NAST has 1084 states. For XRF1-HARW, $n_r = 100$ was selected, which adequately captured the flight dynamics of this very flexible aircraft.

4 MLA SYSTEM DESIGN

The control objective is to perform a prescribed maneuver by tracking command signals while enforcing input and output constraints. In particular, constraints are enforced on the maximum and minimum out-of-plane curvature at the jth selected critical stations for the purpose of MLA:

$$\kappa^j_{x,\min} \leq \kappa^j_x \leq \kappa^j_{x,\max} \tag{36}$$

A reduction in curvature yields a reduction in the out-of-plane bending moment (M_x) at the corresponding station. An integrated flight control and MLA system is then designed to manipulate the aircraft control effectors to achieve such objectives. Figure 3 shows the MPC architecture considered. It is responsible for both command tracking and load alleviation, as discussed in [1]. This work focuses on the MPC design using T2B-ROM, and the observer design is left as future work. In the next derivations, full state feedback is assumed.

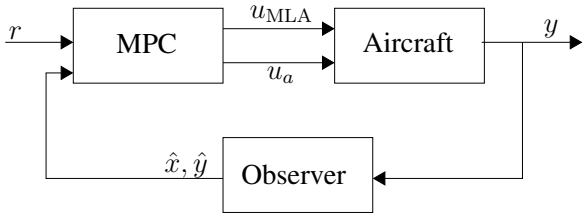

Figure 3: MPC architecture.

The XRF1-HARW model has eleven control effectors available for control design, i.e., outer (u_{oal}, u_{oar}) and inner (u_{ial}, u_{iar}) ailerons at each semi-wing, elevators (u_{el}, u_{er}) at the left and

right horizontal tail planes, a rudder (u_r) at the vertical tail plane, flaperons at the inboard right and left semi-wings (u_{fr}, u_{fl}), and left and right (u_{Tl}, u_{Tr}) point forces acting as thrust. The control surfaces on the wing are shown in Fig. 4a. For control design purposes, the degrees of freedom of the control effectors are reduced to six by imposing the elevators and flaperons to deflect symmetrically ($u_{el} = u_{er} = u_e$ and $u_{fl} = u_{fr} = u_f$), and the inner ailerons to deflect anti-symmetrically ($u_{ial} = -u_{iar} = u_{ia}$). The outer ailerons work independently as elevons. The thrust is assumed constant and, therefore, it is not considered in this flight control system, since it is designed to work at cruise condition.

Two control effector configurations for MLA are considered in here. The first one utilizes only the elevons as the primary control surfaces to perform load alleviation. For this configuration, the following input vectors are defined:

$$\textbf{Configuration 1: } u_{\text{MLA}} = \begin{bmatrix} u_{oal} & u_{oar} \end{bmatrix}^T, \quad u_a = \begin{bmatrix} u_{ia} & u_e & u_r \end{bmatrix}^T, \quad u = \begin{bmatrix} u_a^T & u_{\text{MLA}}^T \end{bmatrix}^T. \tag{37}$$

The second configuration adds the flaperons to the pair of elevons as the main control surfaces to perform MLA. This design choice aims at reducing the deviation from the desired aircraft trajectory when the MLA system is active. For this configuration, the following input vectors are defined:

$$\textbf{Configuration 2: } u_{\text{MLA}} = \begin{bmatrix} u_{oal} & u_{oar} & u_f \end{bmatrix}^T, u_a = \begin{bmatrix} u_{ia} & u_e & u_r \end{bmatrix}^T, u = \begin{bmatrix} u_a^T & u_{\text{MLA}}^T \end{bmatrix}^T. \tag{38}$$

To design the MLA system, the stations monitored during the aircraft operation have to be selected. Among the stations along the XRF1-HARW wing, tail, and fuselage, some of them develop higher loads during maneuvers. The critical stations were identified through open-loop simulations. The stations shown in Fig. 4b were identified as the critical stations concerning the out-of-plane bending moment.

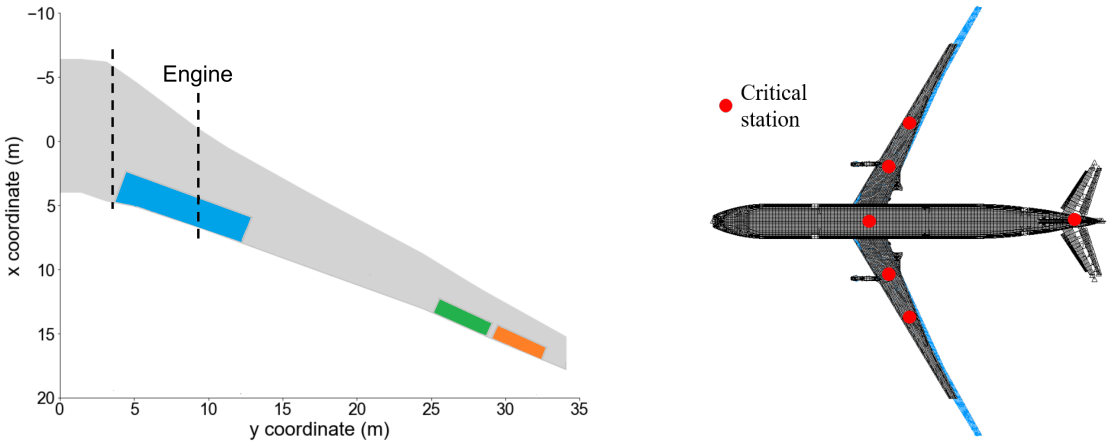

(a) Control surfaces on the wing.

(b) Critical stations (aircrfat in blue).

Figure 4: XRF1-HARW control surface and critical stations layout

For the MPC design, we proceed by converting the T2B-ROM in Eqs. 32-34 to discrete-time assuming a zero-order hold with the sample time of $T_s = 0.02$ s so that the control inputs are constant over each sampling period. The discretization is performed for each model $\mathcal{S}_{r,i,j}$. The

resulting discrete-time T2B-ROM has the following form:

$$\delta x_{r,k+1} = \sum_{i=1}^{M} w_i(V_j \delta x_{r,k} + (I + P_j - V_j P_j)x^0, u_k) \left(A^d_{r,i,j}\delta x_{r,k} + B^d_{r,i,j}\delta u_k\right), \tag{39}$$

$$\delta y_k = \sum_{i=1}^{M} w_i(V_j \delta x_{r,k} + (I + P_j - V_j P_j)x^0, u_k) \left(C^d_{r,i,j}\delta x_{r,k} + D^d_{r,i,j}\delta u_k\right), \tag{40}$$

$$j \in \{0, 1, \ldots, M\} \text{ such that } m(x_{r,k}, u_k) = d_j(V_j \delta x_{r,k} + (I + P_j - V_j P_j)x^0, u_k) \tag{41}$$

where the superscript d denotes the corresponding discrete-time matrices.

The tracked outputs, denoted by y^t_k, are a subset of y_k given by

$$\delta y^t_k = \sum_{i=1}^{M} w_i(V_j \delta x_{r,k} + (I + P_j - V_j P_j)x^0, u_k) \left(C^{d,t}_{r,i,j}\delta x_{r,k} + D^{d,t}_{r,i,j}\delta u_k\right), \tag{42}$$

where $C^{d,t}_{r,i,j} \in \mathbb{R}^{n_r \times n_x}, D^{d,t}_{r,i,j} \in \mathbb{R}^{n_r \times n_u}$, $n_r \leq n_y$, contain selected rows of $C^d_{r,i,j}$ and $D^d_{r,i,j}$, respectively. These outputs are to be controlled to set-points $r \in \mathbb{R}^{n_r}$, which are target values in terms of deviations from the trim values. In the application considered in this work, r contains values for the desired pitch rate, side-slip angle and heading angle, i.e.,

$$r = \begin{bmatrix} r_q & r_\beta & r_\psi \end{bmatrix}^T. \tag{43}$$

The tracking error is given by:

$$e_{k+1} = \delta y^t_{k+1} - r \tag{44}$$

$$= e_k + \sum_{i=1}^{M} w_i(V_j \delta x_{r,k} + (I + P_j - V_j P_j)x^0, u_k) \left(C^{d,t}_{r,i,j}\Delta x_{r,k} + D^{d,t}_{r,i,j}\Delta u_k\right), \tag{45}$$

where

$$\Delta x_{r,k} = \delta x_{r,k+1} - \delta x_{r,k}, \quad \Delta u_k = \delta u_{k+1} - \delta u_k. \tag{46}$$

The MPC problem is formulated to minimize the tracking error e_k, the rate of all control inputs Δu_k, and the magnitude of the control inputs used for MLA δu_{MLA} over a prediction horizon of N steps, while enforcing the constrains in Eq. 36 along with other input and output constraints. The optimization problem solved at each MPC step reads as follows:

$$\underset{\{\Delta u_k, \Delta x_{k+1}, \varepsilon_{k+1}\}_{k=0}^{N-1}}{\text{minimize}} \quad J_N = \sum_{k=0}^{N-1} ||e_{k+1}||^2_Q + ||\Delta u_k||^2_R + ||\delta u_{MLA,k}||^2_{R_M} + \mu \varepsilon^2_{k+1} \tag{47}$$

$$\text{subject to:} \quad E\Delta x_k + F\Delta u_k \leq S\varepsilon_k \text{ for } k = 0, \ldots, N-1, \tag{48}$$

$$x^0 = \text{ current full-order state}, \tag{49}$$

$$x_{r,0} = P_j x^0, \tag{50}$$

$$\delta x_{r,0} = P_j(x^0 - \bar{x}), \tag{51}$$

$$u_0 = \text{current control input}, \tag{52}$$

$$\text{Eqs. } 13, 14, 39, 40, 41, 45, 46, \tag{53}$$

where E, F and S are matrices of appropriate sizes to represent the linear constraints, Q, R and R_M are positive definite weighting matrices, $\varepsilon_k \in \mathbb{R}_{\geq 0}$ is a slack variable, and $\mu \in \mathbb{R}_{>0}$ is a penalty parameter. The pair $(\bar{x}, \bar{u})$ represents the initial full-order state and control input.

Since the weights w_i in Eqs. 39-40 depend on $x_{r,k}$, they can vary within the prediction horizon. They are updated according to the nonlinear equations in Eqs. 13-14, therefore, this optimization problem is non-convex. Furthermore, the switching rule in Eq. 41 can be incorporated into the optimization problem as mixed-integer linear inequalities, thus making this optimization problem a mixed-integer nonlinear programming (MINLP) problem. This class of problems is NP-complete, making it hard to be solved in real-time in an application that demands small sampling times such as the control of a VFA.

To circumvent this issue, the MPC problem is reformulated by simplifying the prediction model. The weights w_i are evaluated at the current full-order state and input, and kept fixed over the prediction horizon. In doing so, the equations used for prediction become linear time-invariant (LTI) models in solving each optimization problem. In addition, the switching rule can be dropped from the optimization problem. The resulting optimization has the following form:

$$\underset{\{\Delta u_k, \Delta x_{k+1}, \varepsilon_{k+1}\}_{k=0}^{N-1}}{\text{minimize}} \quad J_N = \sum_{k=0}^{N-1} ||e_{k+1}||_Q^2 + ||\Delta u_k||_R^2 + ||\delta u_{MLA,k}||_{R_M}^2 + \mu \varepsilon_{k+1}^2 \tag{54}$$

$$\text{subject to:} \quad \delta x_{r,k+1} = \sum_{i=1}^{M} w_i(x^0, u^0) \left(A_{r,i,j}^d \delta x_{r,k} + B_{r,i,j}^d \delta u_k \right), \tag{55}$$

$$\delta y_k = \sum_{i=1}^{M} w_i(x^0, u^0) \left(C_{r,i,j}^d \delta x_{r,k} + D_{r,i,j}^d \delta u_k \right), \tag{56}$$

$$e_{k+1} = e_k + \sum_{i=1}^{M} w_i(x^0, u^0) \left(C_{r,i,j}^{d,t} \Delta x_{r,k} + D_{r,i,j}^{d,t} \Delta u_k \right), \tag{57}$$

$$j \in \{0, 1, \ldots, M\} \text{ such that } m(x^0, u^0) = d_j(x^0, u^0), \tag{58}$$

$$E\Delta x_k + F\Delta u_k \leq S\varepsilon_k \text{ for } k = 0, \ldots, N-1, \tag{59}$$

$$x^0 = \text{ current full-order state}, \tag{60}$$

$$x_{r,0} = P_j x^0, \tag{61}$$

$$\delta x_{r,0} = P_j(x^0 - \bar{x}), \tag{62}$$

$$u_0 = \text{current control input}, \tag{63}$$

$$\text{Eq. 46}. \tag{64}$$

The optimization problem now becomes a quadratic programming (QP) problem, which can be efficiently solved using commercial solvers. The potential prediction errors due to freezing the model over the prediction horizon are mitigated by employing a short prediction horizon, and because MPC is based on a receding-horizon principle, in which only the first move of the optimal sequence $\{\Delta u_k^*\}_{k=0}^{N-1}$ is applied to the plant, i.e.,

$$u_{k+1} = \delta u_k + \Delta u_0^* + \bar{u} = u_k + \Delta u_0^*. \tag{65}$$

In the next MPC step, the prediction model is updated based on the new values of (x^0, u^0), and the same process is repeated recursively.

The QP problem has $N(n_x + n_u + 1)$ decision variables. This number can be reduced to $N(n_u + 1)$ by using Eq. 55 to express Δx_k as a function of Δu_k, therefore eliminating the

decision variables $\{\Delta x_k\}_{k=1}^{N}$ and Eq. 55. A similar procedure can be used to eliminate Eqs. 56 and 57. This process is referred to as condensing. The condensed MPC problem is then a QP problem with only inequality constraints. Because the prediction model is updated at each MPC step, this process has to be repeated whenever the model changes.

5 NUMERICAL SIMULATIONS

In this section, the results of numerical simulations to illustrate the application of the proposed MPC-based MLA system using the T2B-ROM are presented. The objective is to perform the Maneuver Vertical Stretched (MVS) while maintaining the out-of-plane bending (prescribed by the curvatures at the critical stations) within prescribed safety limits. This maneuver consists in, from a leveled flight at 1g condition, applying the following stick trajectory: (i) push the pilot stick with a sine shape until a load factor (n_z) of 2.5g is reached, then (ii) release to turn back to 1g with a sine-like function [6]. To simulate the stick input, an equivalent pitch rate command (Fig. 5a) is fed to the tracking controller described in Section 4, such that the resultant vertical load factor at the aircraft nose follows the desired profile, as shown in Fig. 5b.

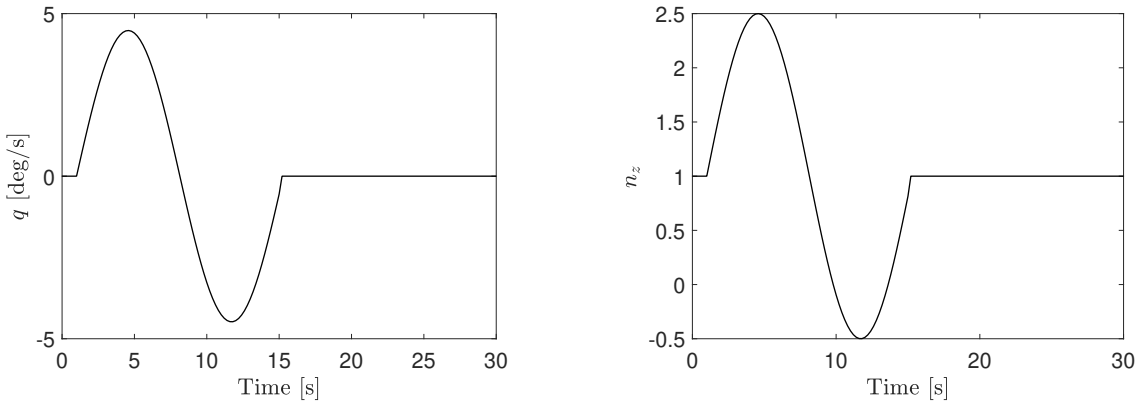

(a) Commanded pitch rate.

(b) Vertical load factor at aircraft nose.

Figure 5: MVS maneuver.

The input and output constraints considered in this example are shown in Tab. 2. The out-of-plane curvature constraints on critical stations on the wing and HTP are defined as an equivalent reduction of approximately 30% from the maximum/minimum peak observed when the MVS maneuver is performed with the MLA system deactivated. The constraints on the control surfaces deflection and rate are in accordance with typical values found in actual large commercial aircraft. The flaperon constraints are only applied in configuration 2 discussed in Section 4. The rate of deflection of this control surface are chosen smaller than the other control surfaces to account for the reduced bandwidth of this type of actuator.

The next XFR1-HARW nonlinear simulations were performed in UM/NAST for configurations 1 and 2 starting at flight condition 54 ($h = 8800$ m and $M = 0.85$). In both cases, the MPC prediction horizon had 50 steps, corresponding to a 1.0 s look ahead into the future. In addition to the results using the T2B-ROM for prediction, simulations were also performed using the linear MPC design, in which the linearized prediction model is fixed at the beginning of the simulation. The computations were performed on a Dell XPS 15 laptop (Intel i7-7700HQ, 2.8GHZ, 16 GB RAM). The controller update was done in MATLAB through the UM/NAST-Controllers MATLAB interface. The QP problem was solved using QPKWIK [7] with warmstarting.

Table 2: Output and input constraints.

Description	Min	Max	Unit
Out-of-plane curvature at critical stations on the wing	-13.5×10^{-4}	4.47×10^{-4}	[1/m]
Out-of-plane curvature at critical stations on the HTP	-1.51×10^{-4}	2.57×10^{-4}	[1/m]
Control surfaces deflection	-25	25	[deg]
Flaperon deflection	-25	25	[deg]
Rate of deflection of control surfaces	-45	45	[deg/s]
Rate of deflection of flaperon	-30	30	[deg/s]

5.1 Configuration 1

In configuration 1, the elevons are used to perform load alleviation while the flaperons are kept at the trim condition. Figure 6 shows the rigid body outputs of XRF1-HARW while performing the MVS maneuver with and without the MLA system. The latter corresponds to the case when the curvature constraints are not enforced and served as a baseline. The structural outputs at selected stations are shown in Fig. 7. The different color intervals shown in the background of each subplot identifies the reduced-order subspace onto which the dynamics was projected. The color code can be read in Table 1. In this example, the subspace was switched ten times in the following order: $\{54, 53, 60, 59, 58, 64, 63, 69, 68, 74, 73\}$.

Even though the out-of-plane curvature constraints on the wing and horizontal tail plane (HTP) were satisfied, the flight control system was not capable of accurately tracking the pitch rate command when these constraints were enforced. A reduction in the pitch rate, with a consequent reduction in the developed pitch angle and load factor, resulted in a deviation from the baseline trajectory, as can be observed in the altitude plot. Nevertheless, reductions of 31.52% in the bending moment on the wing root, and of 42.93% on the HTP root were obtained. The other critical stations on the wing had a similar load reduction, but the constraints did not become active.

The significant trajectory deviation can be explained by the reduction in the elevator input to enforce the MLA constraints, as shown in Fig. 8. For the XRF1-HARW model, the outer elevons alone have low efficacy in reducing the curvature at the wing root, even with large deflections such as the ones observed in this example. Furthermore, they cannot compensate for the loss of pitch rate due to the necessary reduction in elevator input to enforce the HTP constraints, since there are no dedicated MLA control effectors on the tail. Consequently, the elevators play the primary role in reducing maneuver loads, while compromising the tracking performance.

5.2 Configuration 2

The flaperon is added to the set of control effectors dedicated to perform MLA in hopes of minimizing the trajectory deviation. Figure 9 and 10 show the rigid body and structural outputs of XRF1-HARW using configuration 2. In this example, the subspace was switched ten times in the following order: $\{54, 53, 59.58, 64, 63, 62, 68, 67, 73, 79, 85\}$. Now, the pitch rate is close to the reference command, and therefore the pitch angle and altitude have smaller deviations from the baseline values. The vertical load factor follows a similar trend as of the MVS profile, but a peak value of 2.9g is developed instead of the desired 2.5g.

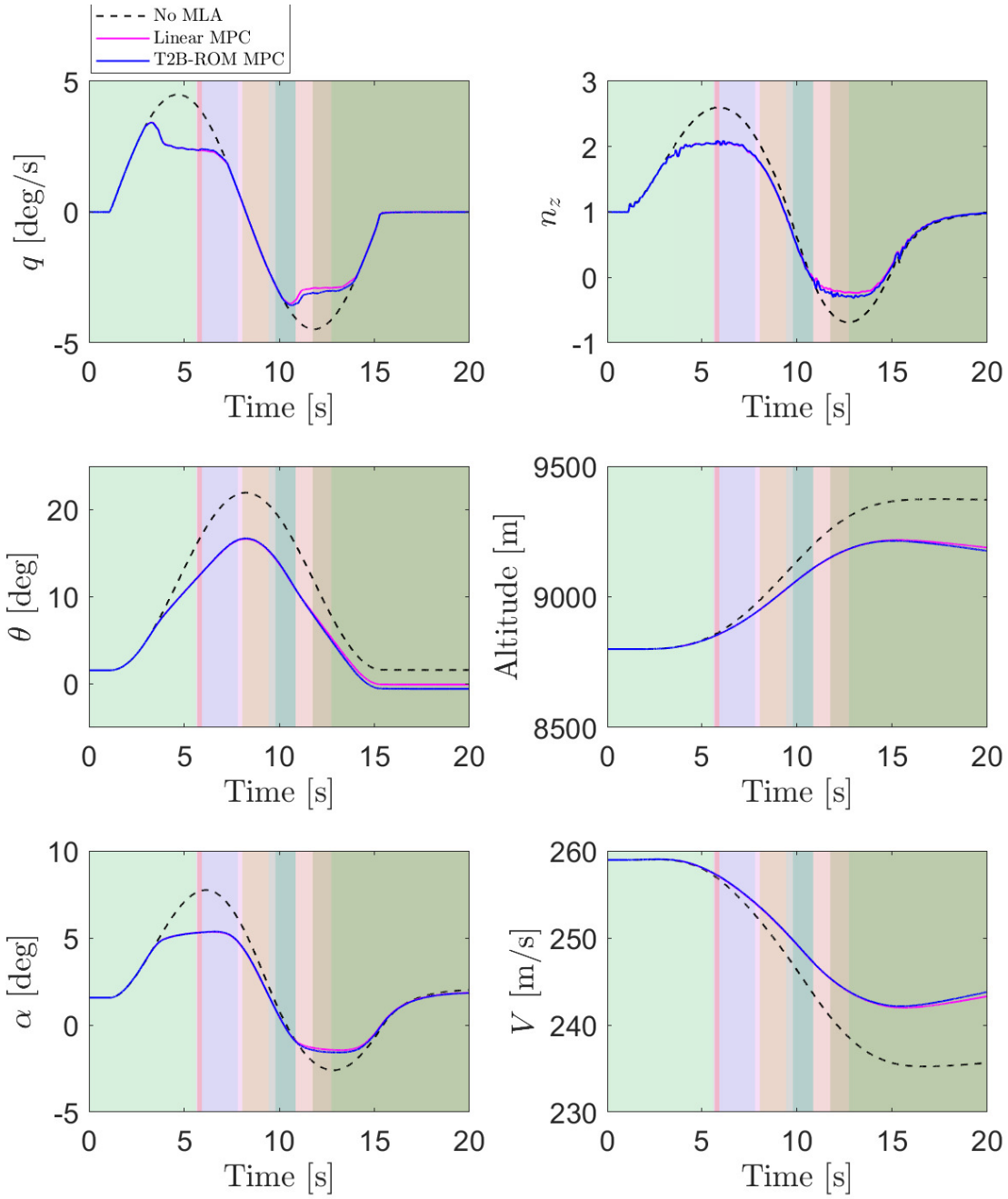

Figure 6: Rigid body outputs of XRF1-HARW using configuration 1 of control surfaces.

The MLA constraints on both wing and HTP critical stations were satisfied. The resulting maximum bending moment alleviation was approximately 36.5% at the wing root, and 21.9% and the HTP root. Similar results were obtained for adjacent critical stations. To achieve such results, the control inputs in Fig. 11 were applied to the vehicle. Note that, despite the fact that the elevator input was reduced, the aircraft was still able to track the pitch rate command by deflecting the flaperons. The coordination between flaperons, elevons, and elevators made possible the achievement of both tracking and load alleviation objectives, in contrast to the results of configuration 1. However, the demanded flaperon deflection is somewhat large, even though the elevon deflections are now smaller, which can cause an increase in drag.

In both configurations, the MPC controller designed with the T2B-ROM had a similar performance as the standard linear MPC design with a fixed prediction model. Some marginal

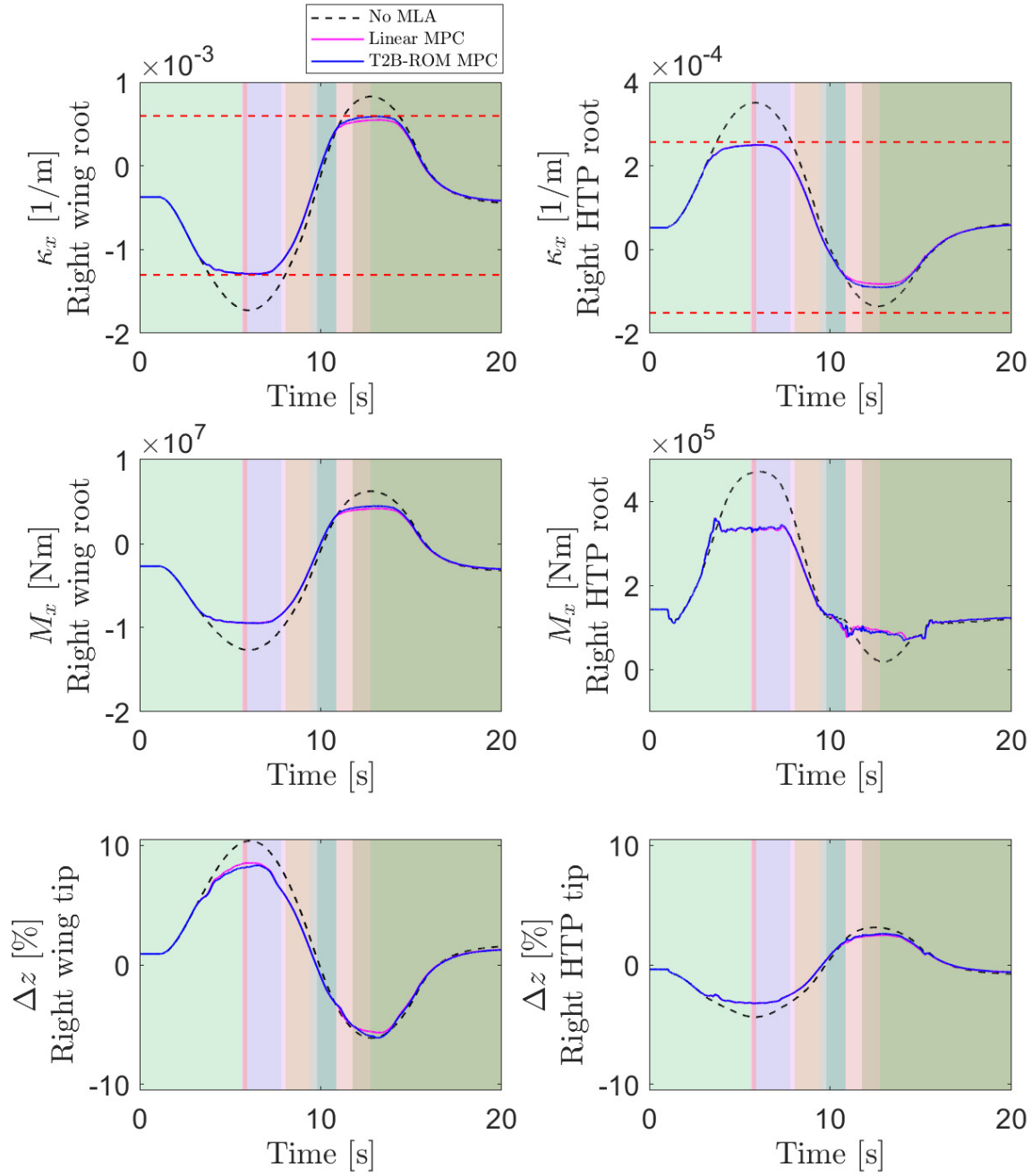

Figure 7: Structural outputs of XRF1-HARW using configuration 1 of control surfaces. κ_x: out-of-plane curvature, M_x: out-of-plane moment, Δz: vertical deflection.

benefits of the T2B-ROM prediction model can be observed in a slightly better signal tracking performance (Fig. 6), a lesser conservative constraint satisfaction (Figs. 7 and 10), and smaller control inputs (Figs. 8 and 11). It is worth noting that in both cases the wing and HTP tip displacements, as shown in Figs. 7 and 10, were smaller than 10%, indicating that the MVS maneuver may not sufficiently excite geometric nonlinear effects that would justify the use of the T2B-ROM.

On the downside, the MPC design with the T2B-ROM has a considerably higher computational cost. Table 3 shows a comparison between the maximum and average computation time of an MPC step for the design with a fixed linear model and the T2B-ROM. This substantial increase

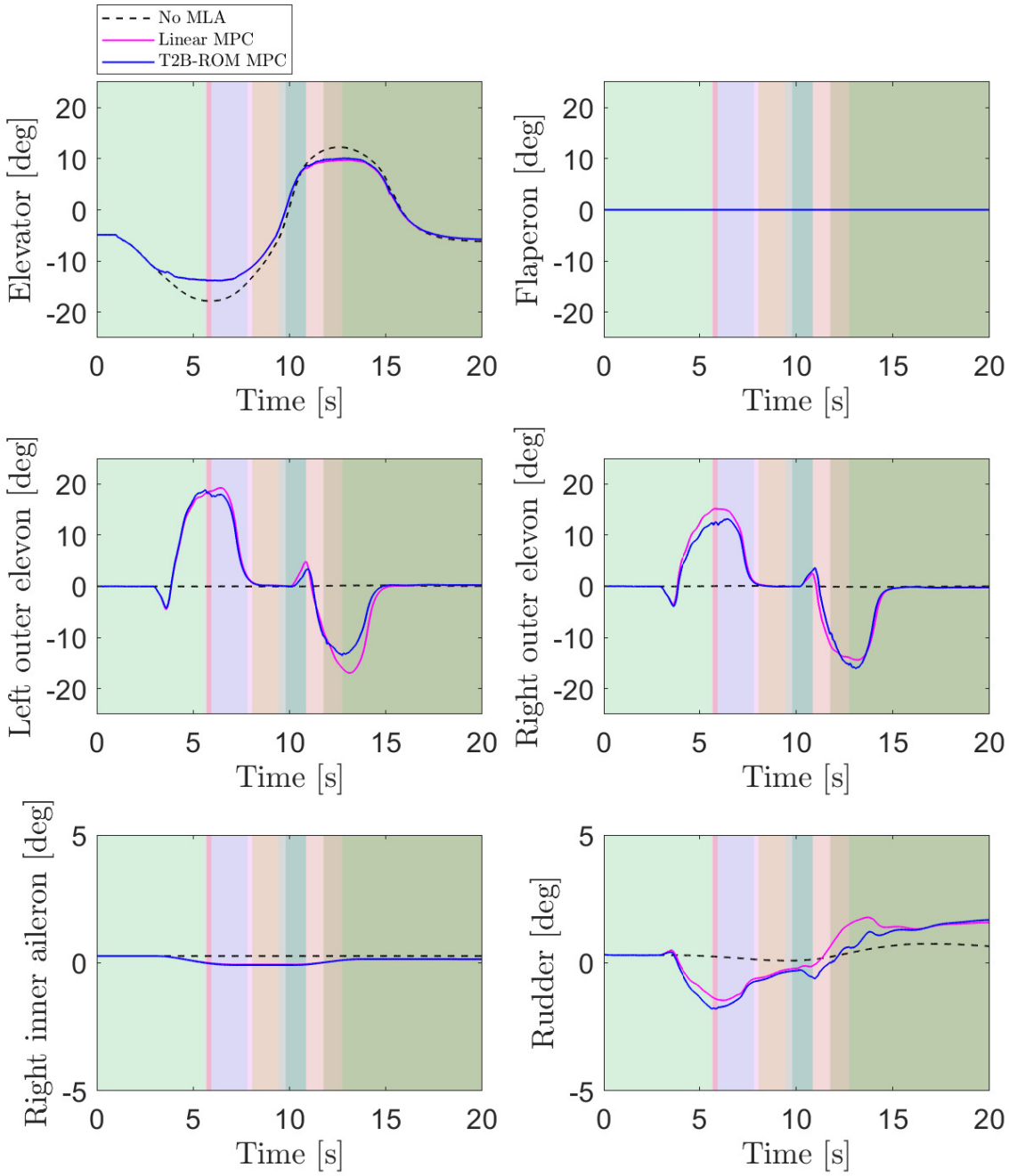

Figure 8: Control inputs applied to XRF1-HARW using configuration 1 of control surfaces.

is due to the necessity of updating the T2B-ROM model at each MPC iteration, in addition to the condensation process, as discussed in Section 4. For the standard linear MPC design, these computations are done offline, thus making it more attractive to real-time implementations.

Table 3: MPC step computation time.

	Max. [s]	Avg. [s]
Linear MPC	0.3082	0.0319
T2B-ROM MPC	21.99	7.762
Augmentation factor	74.4	243

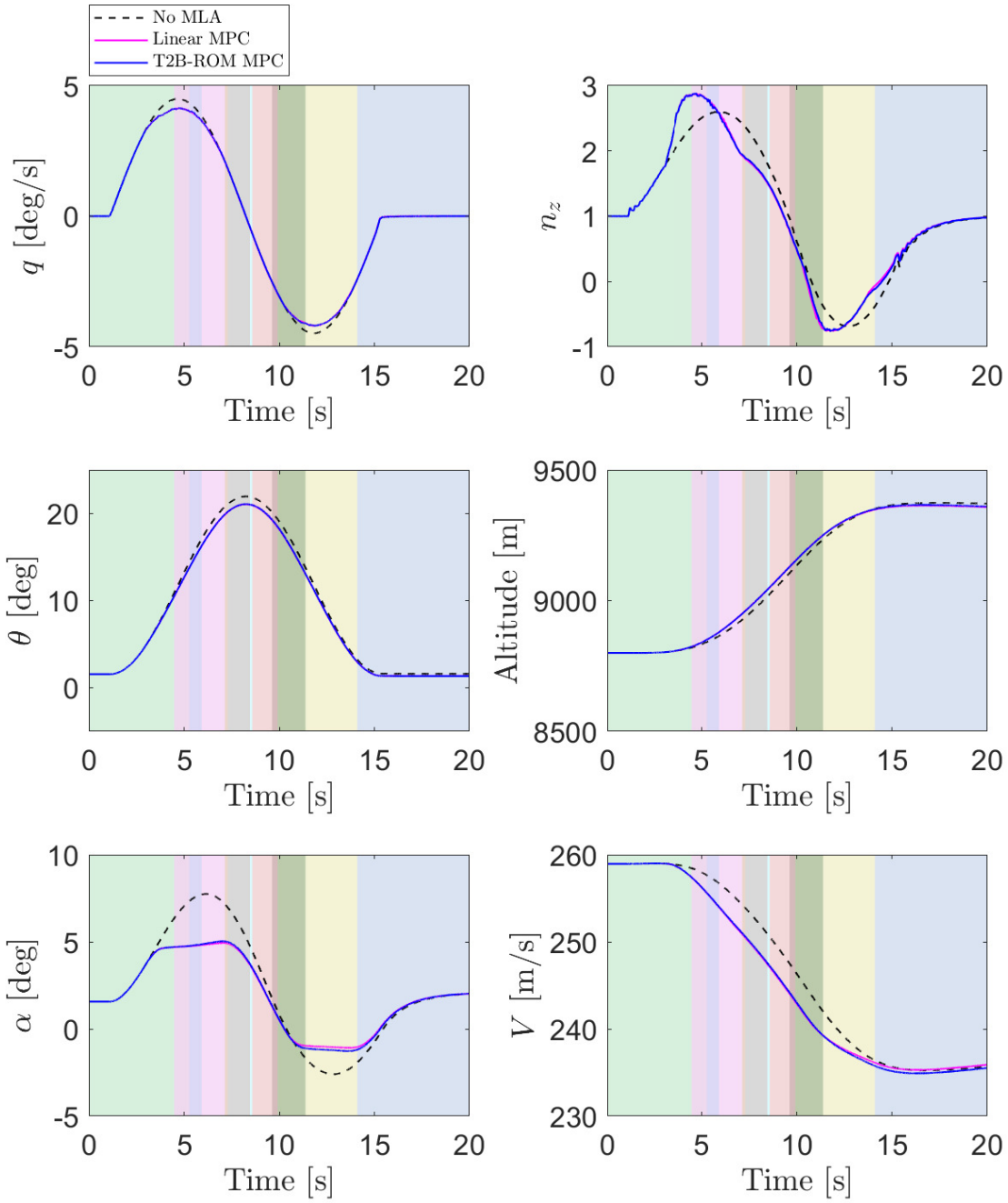

Figure 9: Rigid body outputs of XRF1-HARW using configuration 1 of control surfaces.

6 CONCLUDING REMARKS

This paper presented the design of an MPC-based MLA system for a VFA using a top-to-bottom reduced-order model (T2B-ROM). The model construction and controller design were discussed. Nonlinear numerical simulations were performed using the a very flexible aircraft model with two different control surface configurations.

The results showed that the T2B-ROM provides a good prediction model for MPC design, with smooth transitions between the reduced-order subspaces. However, for the MVS maneuver, the T2B-ROM provided marginal benefits in comparison with the standard design with a fixed linear model. These benefits were overshadowed by the considerably higher cost of the MPC

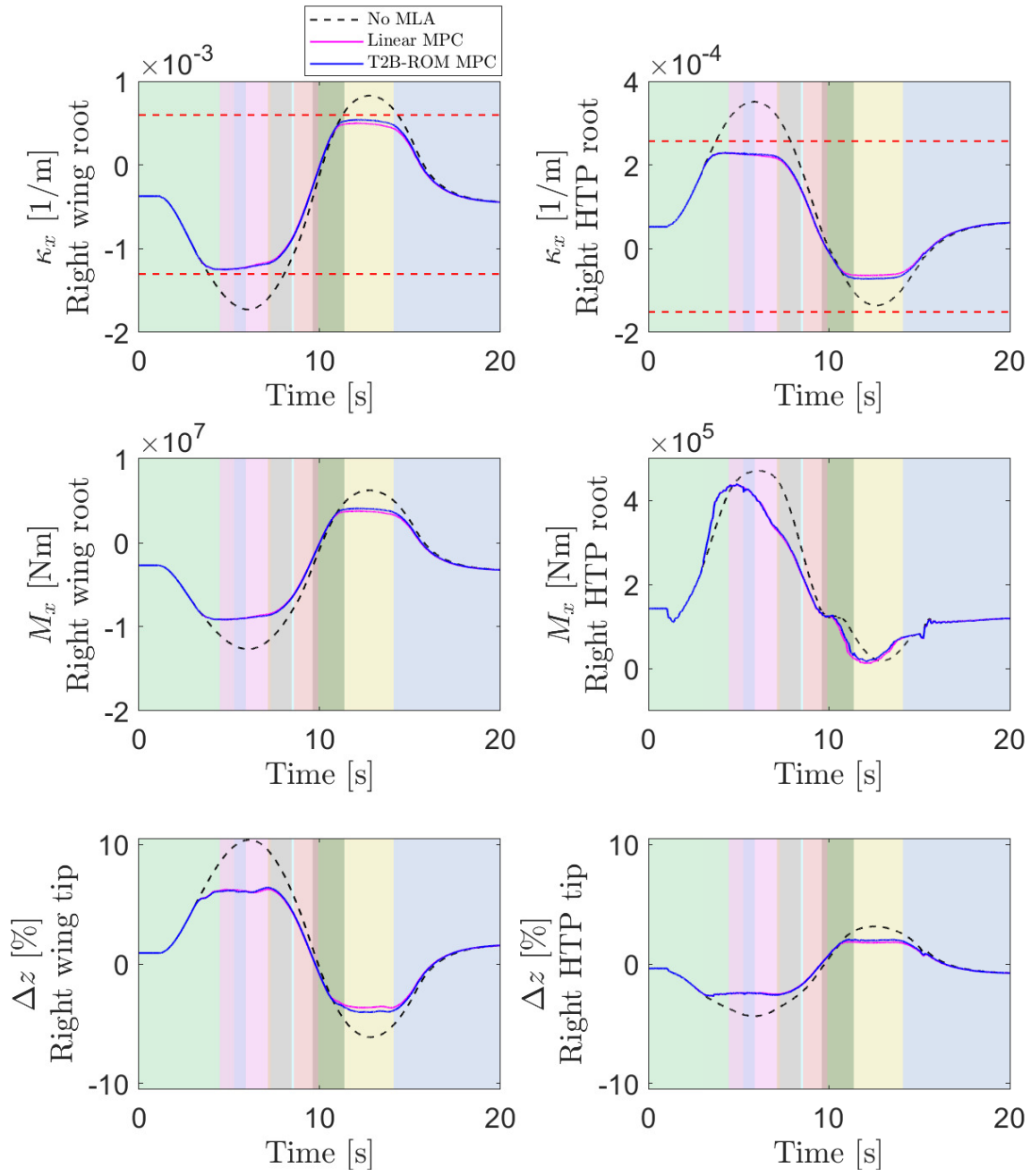

Figure 10: Structural outputs of XRF1-HARW using configuration 1 of control surfaces. κ_x: out-of-plane curvature, M_x: out-of-plane moment, Δz: vertical deflection.

implementation with the T2B-ROM. It seems that it is advantageous to build the prediction model at the starting flight condition and keep it constant for the entire maneuver in order to avoid excessive computations on the fly. Note, however, that this conclusion is based on the results for the MVS maneuver, which does not excite significant geometric nonlinear effects nor changes in flight conditions. Further studies are needed to assess the performance of these MPC designs in more aggressive maneuvers.

Furthermore, the T2B-ROM for VFA could potentially benefit from having the structural deformation as part of the definition of the flight conditions for linearization. This would capture, in addition to the influence of dynamic pressure, the geometric nonlinearities that are more pronounced in this type of aircraft.

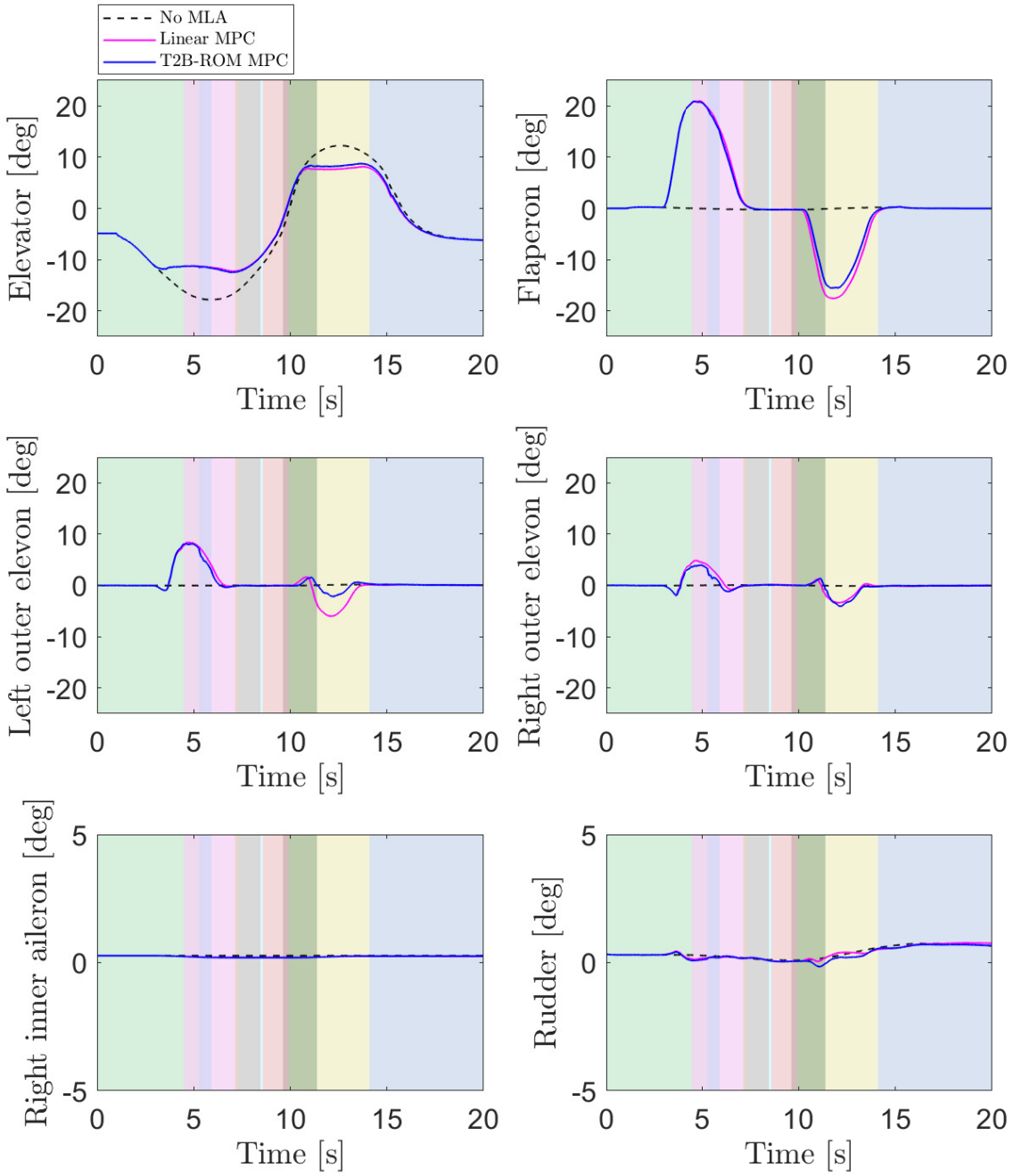

Figure 11: Control inputs applied to XRF1-HARW using configuration 1 of control surfaces.

A combination of several control surfaces distributed along the wing trailing edge seem to be beneficial to the task of alleviating maneuver loads while minimizing trajectory deviations. The outer ailerons alone are ineffective in controlling the curvature on inboard stations. The optimal distribution of such control surfaces can be determined as a solution to an optimization problem with MLA metrics.

Further studies are needed on the reduction of the computational cost to update the T2B-ROM at each MPC iteration. In addition, MPC implementations that exploit the sparsity of the problem can be investigated as an alternative to the condensation process.

ACKNOWLEDGMENTS

The authors would like to thank Airbus for providing the XRF1 test case as a mechanism for demonstration of the approaches presented in this paper. The material of this paper is based upon work supported by Airbus in the frame of the Airbus-Michigan Center for Aero-Servo-Elasticity of Very Flexible Aircraft.

REFERENCES

[1] Pereira, M. F. V., Kolmanovsky, I., Cesnik, C. E. S., and Vetrano, F., "Model Predictive Control Architectures for Maneuver Load Alleviation in Very Flexible Aircraft," *AIAA SciTech 2019 Forum*, San Diego, USA, 2019, p. 1591.

[2] Pereira, M. F. V., Kolmanovsky, I., Cesnik, C. E. S., and Vetrano, F., "Model Predictive Control for Maneuver Load Alleviation in Flexible Airliners," *International Forum on Aeroelasticity and Structural Dynamics - IFASD*, Savannah, Georgia, 2019.

[3] Lanchares, M., Kolmanovsky, I., Cesnik, C. E. S., and Vetrano, F., "Model Order Reduction for Coupled Nonlinear aeroelastic-flight Mechanics of Very Flexible Aircraft," *International Forum on Aeroelasticity and Structural Dynamics - IFASD*, Savannah, Georgia, 2019.

[4] Riso, C., Sanghi, D., Cesnik, C. E., Vetrano, F., and Teufel, P., "Parametric Roll Maneuverability Analysis of a High-aspect-ratio-wing Civil Transport Aircraft," *AIAA Scitech 2020 Forum*, 2020, p. 1191.

[5] Su, W. and Cesnik, C. E. S., "Strain-based Geometrically Nonlinear Beam Formulation for Modeling Very Flexible Aircraft," *International Journal of Solids and Structures*, Vol. 48, 2011, pp. 2349 – 2360.

[6] Burlion, L., Poussot-Vassal, C., Vuillemin, P., Leitner, M., and Kier, T., "Longitudinal Manoeuvre Load Control of a Flexible Large-Scale Aircraft," *Proceedings of the 19th World Congress - The International Federation of Automatic Control (IFAC)*, Vol. 19, IFAC, Cape Town, South Africa, Aug. 2014, pp. 3413–3418.

[7] Schmid, C. and Biegler, L., "Quadratic Programming Methods for Reduced Hessian SQP," *Computers & Chemical Engineering*, Vol. 18, 1994, pp. 817–832.

COPYRIGHT STATEMENT